Motion Planning of Planar Close-Chain Mechanisms With Structural Information

G.F. Liu J.C. Trinkle Y. Yang* Y.G. Chen Xin Chen

***Abstract*—This paper investigates the motion planning problem of planar m-link closed-chains with (point or convex non-point) obstacles. The configuration space (C-space) of closed-chains is embedded into two copies of $m-3$ dimensional torii. The boundary varieties (C-boundaries) of the C-space are sets of configurations where a pair of links overlaps. They not only determine the portion of the aforementioned torii on which the loop can be closed, but also provide necessary transitional configurations from one torus to the other. By dilating each workspace obstacle and sampling the resulting boundaries by a set of points (called dilated point obstacle set), the original configuration space obstacles (C-obstacles) are contained in the union of the semi-algebraic sets cut out by the C-obstacles of the dilated point obstacle set (called dilated C-obstacles). It turns out that the C-boundaries and the dilated C-obstacles contain essential structural information about the connectivity of the collision-free portion of C-space (C-free), which allows us to propose an explicit version of exact cell decomposition and roadmap algorithm specifically for planar closed-chains, along with an efficient sampling-based roadmap algorithm. Simulation results along with animation videos and source codes are provided which demonstrate the effectiveness of our method.**

Kewords- Path planning, closed chains, boundary variety, C-space, C-obstacle, C-free, sampling algorithm.

I. Introduction

Closed-chain manipulators and mechanisms have recently received lots of interests because of their potential advantages over their serial counterparts. They have appeared in many application domains, including parallel machining tools, multipod robots, spatial robotic arms, and humanoids. However, their closed-loop structure gives rise to joint variable dependencies, which manifest in a topologically complex configuration space. An important consequence of this is that, in general, the C-space cannot be globally (and smoothly) parameterized by a single set of d variables (for example a subset of the joint displacements), where d is the number of degrees of freedom (DOFs) of the manipulator. In other words, any d-dimensional atlas of the C-space will contain multiple charts. This fact generally makes motion planning more challenging for closed-chain manipulators than it is for serial manipulators.

A. Previous Work

It is well known that general exact motion planning algorithms for serial manipulators are highly complex [5]–[8], [16]. In fact, the most efficient exact planning algorithm is Canny's, whose worst-case time complexity is exponential in the dimension of C-space [6]. In principle, exact algorithms can be applied to systems with holonomic equality constraints such as those imposed by the kinematic loops in closed-chain manipulators "by defining convenient charts and managing them" (see [7], page 411). However, the difficulty of implementing exact algorithms for general systems fueled a paradigm shift to sampling-based algorithms [9]–[11].

Sampling-based algorithms build a graph that approximates the global structure of C-free. The graph has nodes that correspond to selected points of C-free and arcs between nodes that indicate path connectedness between the corresponding points. The graph can be thought of a network of highways, or a roadmap, of C-free. The roadmap becomes suitable for motion planning when the following two attributes are attained: (1) there is a one-to-one correspondence between components of the graph and those of C-free, and (2) given an arbitrary point in C-free, it is easy to find a path connecting it to the graph. At this point, motion planning is essentially reduced to graph searching.

Sampling-based algorithms have been quite successful for systems whose C-space can be parameterized by a single chart with number of coordinates equal to the DoFs of the system, but less successful otherwise [12], [17]. Even though one can always generate an ambient space parameterizable by a single chart by choosing more parameters than the dimension of C-space, the number of sample points needed to construct a good roadmap grows exponentially with the dimension of the ambient space, because the number of connected components of C-free of this space grows exponentially with its dimension and often a large portion of the ambient space is unaccessible.

To handle this difficulty, Yakey, LaValle, and Kavraki [12] proposed to sample points on the embient space first, and then pull them back to the submanifold by applying an optimization algorithm that closes the loop gap. However, the algorithm might take long time to converge for some samples in the embient space. Kim et al. [22] devised a different algorithm that samples the tangent bundle of the C-space submanifold along with a method for quick projection from the tangent bundle to the submanifold.

Second, for most closed-chain manipulators of interest, parametrization of C-space using the minimal number of coordinates requires multiple charts. These can be difficult to define and to choose suitable metrics to obtain globally "well distributed" sample points. There exists singular loci in C-space pertained to any local coordinate chart [23]–[25]

which are crucial for establishing the adjacency between different charts. Traditional sampling-based approach will often predict wrong results if none of these critical configurations gets sampled. The same phenomenon was also observed in reconfigurable parallel robots with multiple motion branches [26], [27]. Although the RLG method [13] provides partial remedies to traditional algorithms by estimating the motion range of each joint of the linkage that obeys the loop closure constraint, the algorithm fails to sample the singular loci and narrow passages, and thus may give a wrong answer for some path queries.

The difficulties associated with applying sampling-based motion planning methods to closed-chain manipulators and the availability of new results in topology led to renewed interest in exact planning algorithms for closed kinematic chains (see Fig. 1) [18]–[20]. Trinkle and Milgram derived some global topological properties of the C-space (the number of components and the structures of the components) of single-loop closed chains with spherical joints in a workspace *without* obstacles [18]. They show that the C-space is the union of manifolds that are products of spheres and intervals. An efficient path planning algorithm can be carried out by iteratively moving those joints corresponding to the spheres to their goals, while the remaining links follow accordingly so that the loop can be closed.

The planning algorithm for closed chains in [18] was not designed to handle obstacles. In [19], [20], point obstacles were added to the workspace of a planar manipulator, but the closed chain constraint was relaxed. The C-obstacles were analyzed in detail, to reveal that C-free locally fibres over a lower-dimensional base manifold with fibers composed of open intervals. C-free is given by gluing these intervals together. The connectivity of C-free is essentially determined by the critical points where these fibers bifurcate.

B. Contribution

In this paper, the methods used in [18]–[20] are brought together to design a modified version of the existing cell decomposition and the (exact and sampling-based) road map algorithms for an m-link planar closed chain moving among obstacles. The main steps are

1) Partition C-space into two pieces embedded in two (m-3)-dimensional tori;
2) Compute/sample the boundaries of the loop closure constraint variety[1] to identify the reachable portions of C-space;
3) Compute/sample the regions near each C-obstacle in each torus through a dilated point obstacle set;
4) Construct a connectivity graph of C-free based on computed C-boundaries and C-obstacles.

The key steps of our approach are Step 2 and 3. The boundary variety plays an important role in bridging the two pieces of C-space embedded in the two (m-3)-dimensional tori, and identifying their reachable portions. Regions near collision varieties are essential for finding possible narrow passages among C-obstacles.

[1]An algebraic variety in $\mathbb{R}^n$ with coordinates $(x_1, \cdots, x_n)$ is defined as the set of points satisfying a system of polynomial equations $f_i(x_1, \cdots, x_n) = 0$, $i = 1, \cdots, k$.

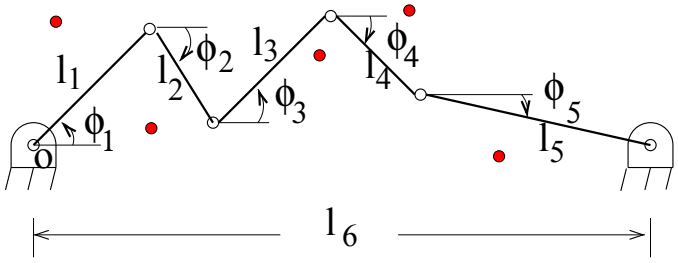

Fig. 1. A closed 6-chain among point obstacles (shown as small discs).

In our approach, the structure of the boundary varieties as well as collision varieties is obtained via analyzing the C-spaces of a set of recursively constructed planar closed chains.

II. Basic notation and terminology

Imagine a planar serial chain of $m-1$ links connected by revolute joints, with one end free, and the other connected to the ground. The ground is regarded as link m and is referred to as the base of the chain. Relative to the base, the open chain has $m-1$ degrees of freedom and its C-space is simply a product of $m-1$ circles, (*i.e.*, $\mathcal{C} = (S^1)^{m-1}$). A closed m-chain can be constructed by attaching the distal end of the open chain to the base as shown in Fig. 1. Mathematically, this attachment imposes two algebraic equality constraints, causing the C-space of the closed chain to become a compact, closed, real, variety of dimension $m-3$. This variety is a manifold as long as the distance between the two base connections is not equal to one of the 2^{m-2} critical lengths [18].

To fix notation, let $\{l_1, \cdots, l_m\}$ denote the fixed link lengths and $\{\phi_1, \cdots, \phi_m\}$ denote their angles measured counterclockwise from the vector from the center of joint 1 to the center of joint m. Thus ϕ_m is always equal to π.

Suppose that there is a finite set $\mathcal{O}$ of point obstacles $\{p_1, \cdots, p_n\}$ that the closed m-chain may not touch. The set of configurations for which a link intersects a point obstacle forms an arrangement of (m-4)-dimensional varieties. The union of these varieties is the C-obstacle $\mathcal{C}_{\text{obst}}$. If link-link collisions are also to be avoided, $\mathcal{C}_{\text{obst}}$ becomes the union of the (m-4)-dimensional collision varieties and an (m-3)-dimensional link-link collision set. C-free, denoted by $\mathcal{C}_{\text{free}}$, is the compliment of $\mathcal{C}_{\text{obst}}$ in $\mathcal{C}$.

Finally, the path planning problem can be stated as follows: given $\phi_{\text{init}} = (\phi_1, \cdots, \phi_m)_{\text{init}} \in \mathcal{C}_{\text{free}}$ and $\phi_{\text{final}} = (\phi_1, \cdots, \phi_m)_{\text{final}} \in \mathcal{C}_{\text{free}}$ determine a continuous map $\tau \in [0,1] \mapsto (\phi_1(\tau), \cdots, \phi_m(\tau)) \in \mathcal{C}_{\text{free}}$ such that $\phi(0) = \phi_{\text{init}}$ and $\phi(1) = \phi_{\text{final}}$, or report that no such path exists.

III. C-space of Planar Closed Chains

Here we summarize three results from topological approaches to motion planning that are crucial to the work

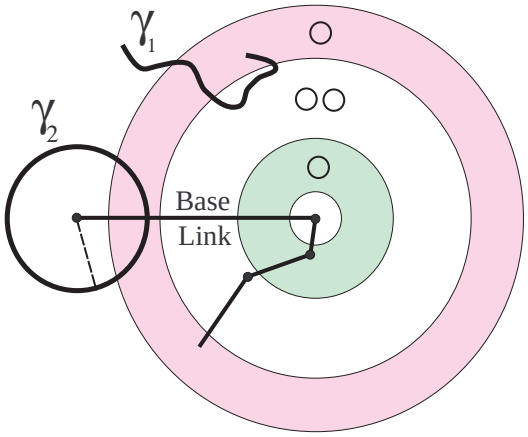

Fig. 2. Construction of C-space of closed chains via singular circles of an open chain.

presented here. The first result is about the connectivity of $\mathcal{C}$ of a planar closed chain. We need a concept called "long links" [18] which is defined as a subset $\mathcal{L}$ of the links such that the sum of the lengths of every pair of distinct links in $\mathcal{L}$ is strictly greater than half of the sum of the lengths of all m links. Note that $\mathcal{L}$ may not be unique. Let $\mathcal{L}^\star$ be a set with maximal cardinality. Then the number of "long links" of a closed chain is defined as $|\mathcal{L}^\star|$. Due to the strict inequality in the definition, the number of long links $|\mathcal{L}^\star|$ must be 0, 2, or 3. If $|\mathcal{L}^\star|$ is equal to 3, $\mathcal{C}$ has two components; otherwise, it has one.

The second result gives the topology of $\mathcal{C}$. It says that for given lengths $\{l_1, \cdots, l_{m-1}\}$ and base length l_m that is generic with respect to those $m-1$ lengths, $\mathcal{C}$ is the boundary of a manifold with boundary, which is given as the union of sub-manifolds of the form $(S^1)^k \times I^{m-2-k}$ [18], where I^d denotes the interval of dimension d.

To clarify the above conclusion, consider Fig. 2, which shows a horizontal base link and three moveable links anchored at the center of four concentric circles. These circles are the singular circles (not drawn to scale) of the open 3-chain. If the end point of the 3-chain is anchored at any point it can reach, its C-space $\mathcal{C}$ is that of a closed 4-chain. If the anchor point is on one of the singular circles, the three links in the chain can be arranged to be colinear and $\mathcal{C}$ is either a single point or a figure eight, while if the anchor point is interior to one of the three reachable annuli, then $\mathcal{C}$ is one circle or two disjoint circles (as indicated by the small circles at the 12 o'clock position of the concentric circles).

Assume that the end point of the open 3-chain is constrained to a one-dimensional curve γ. This effectively converts the open chain into a closed chain whose C-space can be constructed by "gluing" together all the C-spaces at each point as we move along γ. For example, begin at the left end of curve γ_1 and traverse it to its other end. Initially, the C-space over each point of γ_1 is empty, since the open 3-chain cannot reach those points. At the intersection with the outer-most circle, $\mathcal{C}$ of the closed chain is a point, but the workspace segment lying inside the outer-most annular region generates a tube. At the point where γ_1 intersects the next singular circle, $\mathcal{C}$ of the closed 5-chain is a figure eight. This signifies a bifurcation of the tube into two tubes. The two tubes coalesce into a single tube at the next crossing of the same singular circle. Finally, at the end of the curve, $\mathcal{C}$ is a circle. Thus $\mathcal{C}$ of the mechanism with the end of the open 3-chain constrained to lie on γ_1 is a tube pinched closed at one end, open at the other, and with a hole through the tube somewhere between the two ends. Applying the same logic to the closed 5-chain that would result from connecting the end of the open 3-chain to the link shown as a dashed line, one finds that $\mathcal{C}$ of the closed 5-chain is a sphere. This result shows that $\mathcal{C}$ of an m-link closed chain can be obtained by gluing the C-spaces of $(m-1)$-link closed chains in a recursive manner.

The third result pertains to the parametrization of $\mathcal{C}$. Since $\mathcal{C}$ of a generic closed m-chain is an (m-3)-dimensional manifold, it can be locally parameterized by a set of $m-3$ joint angles. However, fixing the orientations of $m-3$ links (including the fixed base angle) does not fix the configuration of the closed chain. Returning to Fig. 1, fixing ϕ_3, ϕ_4 and ϕ_5 still allows *elbow-up* and *elbow-down* postures of links 1 and 2.

This last result suggests partitioning $\mathcal{C}$ into an *elbow-up* piece and an *elbow-down* piece as follows. Break the closed chain at the third joint, thus creating an open 2-chain and an open (m-3)-chain based at opposite ends of the base link. The C-space of the second open chain is the (m-3)-dimensional torus. For an arbitrary point in this space, the chain can be closed in 0, 1, or 2 configurations of the 2-chain. When there are two configurations, they are labeled *elbow-up* and *elbow-down*. Since there are never more than two configurations that close the loop, two copies of the torus suffice to represent $\mathcal{C}$ of the closed chain. When there is only one configuration, the *elbow-up* and *elbow-down* configurations have converged, so at these points, the tori are connected. These configurations form a variety referred to as the *boundary variety* that is the subject of the next section.

IV. Boundary Variety and Its Combinatorial Structure

In this section, we outline a recursive projection method (similar to the approach in [19] and [20]) to determine the structure of the boundary variety. The k^{th} level of recursion will be denoted by appending "(k)" to the expression in question. Refer to Fig. 1. As described above, let us break the closed m-chain into an open 2-chain $\text{CH}_1(1)$ with link lengths $\{l_1, l_2\}$, and an open (m-3)-chain $\text{CH}_2(1)$ with link lengths $\{l_3, \cdots, l_{m-1}\}$ based at the point $(l_m, 0)$. Choose the joint angles of $\text{CH}_2(1)$ as the parameterization of the *elbow-up* and *elbow-down* tori. Further, let $f_{2,1}$ be the forward kinematic map of $\text{CH}_2(1)$.

The boundary variety $B(1)$ is the set of all configurations for which the endpoints of the two open chains can be

connected when the links of the open 2-chain are collinear. With the constraint of collinearity, the space of possible end point locations $\Sigma(1)$ of the 2-chain in the workspace is a pair of concentric circles of radii $l_1 + l_2$ and $|l_1 - l_2|$ centered at the origin. The boundary variety can now be defined as follows:

$$B(1) = f_{2,1}^{-1}(\Sigma(1)).$$

Note that $B(1)$ is the union of the C-space of the two closed (m-1)-chains $M_1(1)$ and $M_2(1)$ with link lengths $\{l_1+l_2, l_3, \cdots, l_m\}$ and $\{|l_1-l_2|, l_3, \cdots, l_m\}$. Also, $B(1)$ is empty if and only if the intersection between $\Sigma(1)$ and the annulus centered at $(l_m, 0)$ with radii $\sum_{i=3}^{m-1} l_i$ and $\min(\|l_3 \pm \cdots \pm l_{m-1}\|)$ is empty, in which case, $\mathcal{C}$ is not connected.

The process described above is repeated for each of the two closed (m-1)-chains. That is, each of these closed chains is assumed to have their third joints removed, which gives rise to 2^2 singular circles centered on the origin with radii $|l_1 \pm l_2 \pm l_3|$ and whose union is $\Sigma(2)$. Similar to $B(1)$, the boundary variety $B(2)$, is given as $B(2) = f_{2,2}^{-1}(\Sigma(2))$, where $f_{2,2}$ is the forward kinematic map of the $\{l_4, \cdots, l_{m-1}\}$ open (m-4)-chain $\mathrm{CH}_2(2)$ based at the point $(l_m, 0)$. By construction, it is clear that $B(2)$ is the union of the C-spaces of the four closed (m-2)-chains each with first link length equal to one of the four singular radii. $B(2)$ is also the set of critical values, or skeleton of the projection of $B(1)$ onto the (m-4)-dimensional torus with coordinates $\{\phi_4, \cdots, \phi_{m-1}\}$.

Recursion continues until $B(m-3)$ is defined. In this case, $\Sigma(m-3)$ is the union of 2^{m-3} concentric circles centered at the origin. The boundary variety $B(m-3)$ is the set of values of ϕ_{m-1} where the circle of radius l_{m-1} centered at $(l_m, 0)$ intersects the singular circles comprising $\Sigma(m-3)$. With $\{B(1), \cdots, B(m-3)\}$ defined, $\mathcal{C}$ can now be decomposed into reachable and unreachable cells which are (m-3)-dimensional cylinders.

Example: Consider a closed 6-chain, with link lengths, $\{0.5512, 1.9457, 1.2131, 2.9482, 4.5684, 5.7815\}$. The C-space of this chain is connected, since there are only two long links. It is contained in two three-dimensional tori that are connected through the boundary variety $B(1)$. $B(1)$ is the union of the C-spaces of two closed 5-chains $M_1(1)$ and $M_2(1)$ with the last four link lengths $\{1.2131, 2.9482, 4.5684, 5.7815\}$ and the first link of length equal to one of the critical lengths $\{1.3945, 2.4969\}$ of the circles composing $\Sigma(1)$. Using the approach described in Fig. 2, the C-spaces of each of $M_1(1)$ and $M_2(1)$ is a bitorus, $T^2 \# T^2$. This is consistent with the fact that each of of $M_1(1)$ and $M_2(1)$ have two long links.

To draw $B(1)$, it is convenient to represent a 3-torus as a three-cube with edge length 2π and opposite faces identified. In this space, a bitorus (qualitatively like those composing $B(1)$) is shown in Fig. 3. Note that the bold girth curve and the two circles where the bitorus is cut (recall that the top and bottom circles are identified) is the skeleton of the bitorus under the projection map onto the (ϕ_4-ϕ_5)-space.

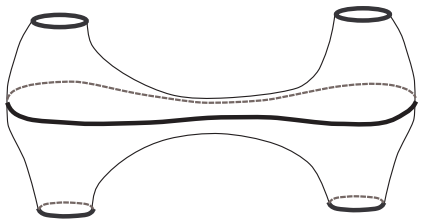

Fig. 3. A bitorus drawn in a cubical representation of C-space. The skeleton of this bitorus under a vertical projection map (drawn bold), is three circles.

$B(2)$ is the skeleton of $B(1)$ under the vertical projection onto the (ϕ_4-ϕ_5)-face of the cube. In Figs. 5 and 6, $B(2)$ is plotted in thin solid closed curves. Note that $B(2)$ consists of six circles; two pairs of small "concentric" circles and one pair of large concentric circles containing the other two pairs. The large circles are the projections of the girth curves of the bitori of $B(1)$. The two pairs of small circles are the small circular skeletal curves like those shown in Fig. 3. The fact that these pairs of circles are concentric implies that the two bitori of $B(1)$ are "nested" in $\mathcal{C}$.

The last step is to project the skeleton of $B(2)$ to an edge of the cube. This is shown by the 12 dashed vertical lines (three are covered by other vertical lines) in Figs. 5 and 6. Using the approach discussed in Fig. 2, one can show that six of the eight singular circles with the radii $\{6.6582, 5.5558, 4.2320, 3.1296, 2.7668, 1.6644\}$ are intersected transversally by the workspace of the end point of the open 1-chain $\mathrm{CH}_2(3)$. These correspond to the 12 critical values of ϕ_5.

V. Collision Varieties and Their Combinatorial Structures

Let $V_{p_i}^j$, $j = 1, \cdots, m-1$, denote the (m-4)-dimensional variety corresponding to p_i lying on link j. The union of these varieties over all links gives the contribution of p_i to the C-obstacle:

$$V_{p_i} = \bigcup_{j=1}^{m-1} V_{p_i}^j.$$

The union of the V_{p_i} over all point obstacles in $\mathcal{O}$ is denoted by V:

$$V = \bigcup_{i=1}^{n} V_{p_i}.$$

To study the global structure of these varieties, the closed chain is again broken into the open 2-chain $\mathrm{CH}_1(1)$ and the open (m-3)-chain $\mathrm{CH}_2(1)$. Consider first $V_{p_i}^j$ for $j = m-1, \cdots, 3$, and $i = 1, \cdots, n$, which can be viewed as the contact varieties of $\mathrm{CH}_2(1)$ clipped by the $B(1)$. The portions of the contact varieties of $\mathrm{CH}_2(1)$ lying on the unreachable side of $B(1)$ are eliminated. Fig. 4 shows a cylinder with rectangular cross section in a three-dimensional C-space. The cylinder is cut by V_{p_1}, V_{p_2} and two patches of $B(1)$, labeled $B(1)(1)$ and $B(2)(1)$.

Assuming the top and bottom of the rectangular column are identified and ignoring $B(1)$, there are two cells in the cylinder. Assuming that the region above the top patch and below the bottom patch of $B(1)$ are unreachable, a portion of V_{p_2} is clipped and there are three cells.

The topological properties of the remaining varieties, $V^1_{p_i}$ and $V^2_{p_i}$, $i = \{1, \cdots n\}$, are determined by the technique developed in [18] and described in the discussion of Fig. 2. These varieties can be expressed as follows:

$$V^1_{p_i} = f^{-1}_{2,1}(\gamma^i_1) \quad (1)$$
$$V^2_{p_i} = f^{-1}_{2,1}(\gamma^i_2) \quad (2)$$

where γ^i_j is the workspace of the end-point (always a closed loop) of $\mathrm{CH}_1(1)$ when link j ($j = 1, 2$) is in contact with p_i. Again it is important to understand the intersection of these contact varieties with $B(1)$. Since the boundary constraint requires links 1 and 2 to be colinear, the intersections of $V^1_{p_i}$ (also $V^2_{p_i}$) with $B(1)$ can be seen to be the C-spaces of two closed (m-2)-chains formed by replacing links 1 and 2 by a single link of length $|l_1 \pm l_2|$ and fixing this link in contact with p_i.

Each collision variety $V^j_{p_i}$ has similar recursive combinatorial structure as the boundary variety $B(1)$. We let $V^j_{P_i}(1)$ denote the variety itself, and $V^j_{p_i}(k)$ the boundary of $V^j_{p_i}(k-1)$ with respect to the projection map $(\phi_{1+k}, \cdots, \phi_{m-1}) \rightarrow (\phi_{2+k}, \cdots, \phi_{m-1})$. It is easy to see that $V^j_{p_i}(k)$ is simply the intersection set between $V^j_{p_i}(k-1)$ and $B(k-1)$. In other words we have the following recursive relation

$$V^j_{p_i}(k) = V^j_{p_i}(k-1) \cap B(k-1), k \geq 2. \quad (3)$$

The intersections between any pair of collision varieties $V^{j_1}_{p_{i_1}} \cap V^{j_2}_{p_{i_2}}$ is given by the set of configurations of the closed chain for which link j_1 and j_2 insect, respectively, the points p_{i_1} and p_{i_2}. Again $V^{j_1}_{p_{i_1}} \cap V^{j_2}_{p_{i_2}}$ has a recursive combinatorial structure, through its recursive intersection with $B(k)$. Similarly one can obtain the structure of the intersection variety $V^{j_1}_{p_{i_1}} \cap V^{j_2}_{p_{i_2}} \cap V^{j_3}_{p_{i_3}}$ as long as it is not empty. In worst case, the number of collision varieties as well as their intersection varieties is $O((nm)^{m-3})$ when $n >> m$. For future development, among all collision varieties and their intersections, those with $m-4$ dimension is put into the set $\Gamma(1)$, and those with $m-5$ dimension into the set $\Gamma(2)$, and so on, until we obtain $\Gamma(m-4)$ which is a one-dimensional set, and $\Gamma(m-3)$, a set of discrete points along ϕ_{m-1} axis.

Example continued: We introduce two point obstacles, $p_1 = (4, 2)$ and $p_2 = (3, 1)$. Note that it is impossible for link 1 or 2 to touch either point, so the corresponding varieties are empty. Consequently, only the contact varieties of links 3, 4, and 5 appear in Figs. 5 and 6. Note that the two thickest vertical lines at $\phi_5 \approx \pm 1.38$, define extreme points of the boundary variety $B(1)$. By these figures, one can also determine the structure of $V^5_{p_i}$, which projects to the two second thickest vertical lines in the figures. Take $V^5_{p_2}$ as an example. The projection of $V^5_{p_2}$ is the line $\phi_5 \approx -0.345$ whose intersection with the interior between the pair of large concentric circles of $B(2)$ is two separated line segments, and with the interior of the inner pair of circles an interval. This reveals that the cross-section of $V^5_{p_2}$ in the horizontal plane of each 3-torus changes from two separated segments to one segment, and then back to two separated segments (recall that opposite faces of each 3-torus are identified). The boundary of the cross-section is either four or two separated points, the union of which gives $B(1) \bigcap V^5_{p_2}$. Gluing the two pieces of $V^5_{p_2}$ in the *elbow-up* and *elbow-down* tori along $B(1) \bigcap V^5_{p_2}$ yields the surface $T^2 \# T^2$. This result can also be obtained using the approach described in Fig. 2 for the corresponding closed 5-chain of $V^5_{p_2}$ with the link lengths {0.5512, 1.9457, 1.2131, 2.9482, 2.1415), which has two long links. Using the same analysis method, we can see that $V^5_{p_1}$ is a torus T^2 (in Figs. 5 and 6, the line of $V^5_{p_1}$ has no intersection with the interior between the inner pair of circles).

VI. Explicit Exact Algorithms

General exact algorithms, including cell decomposition and roadmap algorithms, are often relied on polynomial representation of constraints and computational algebra method. Except for some extremely simple examples (e.g. robots with few DOFs in a workspace with few simple obstacles), these are very hard to make explicit. In this section we employ the structural info of C-free to provide an explicit exact cell decomposition and roadmap algorithm without converting constraints into polynomials.

A. Exact Cell Decomposition Algorithm

The recursive structure of the boundary varieties $\{B(1), \cdots, B(m-3)\}$ provides all the elements for constructing a cylindrical decomposition of the *elbow-up* and *elbow-down* tori. Compared with the general cylindrical cell decomposition algorithm which is based on elimination and projection of semi-algebraic sets, our approach computes the critical sets of each projection map directly from the C-spaces of recursively constructed close-chains. This eliminates the needs to represent the configuration space manifold and collision varieties as semi-algebraic sets, as well as the extra efforts to calculate the critical sets from the semi-algebraic sets.

In essence, the graph construction process is recursive, starting with the one-dimensional circle parameterized by ϕ_{m-1} and working up to the full (m-3)-dimensional C-space. Referring to Fig. 5, the circle in T^2_u parameterized by ϕ_5 has 12 distinct critical points. Removal of these points from the ϕ_5 circle defines a set of 12 open intervals. Some of the two-dimensional cells above these intervals could be disconnected at these critical points, but whether or not this is the case is only revealed as the method proceeds. Therefore, initially, these intervals and the cells above them are assumed to be disconnected at the critical points. Thus, at this stage, the graph of the space of ϕ_{m-1} is simply 12 disconnected nodes. The same decomposition

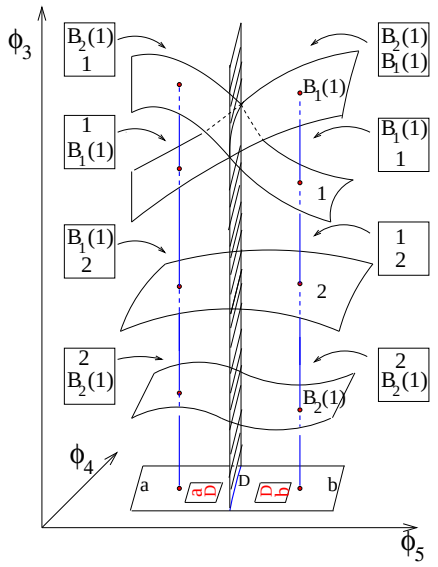

Fig. 4. A rectangular cell in (ϕ_4,ϕ_5)-space onto which the critical points of constraint varieties in (ϕ_3,ϕ_4,ϕ_5)-space are projected.

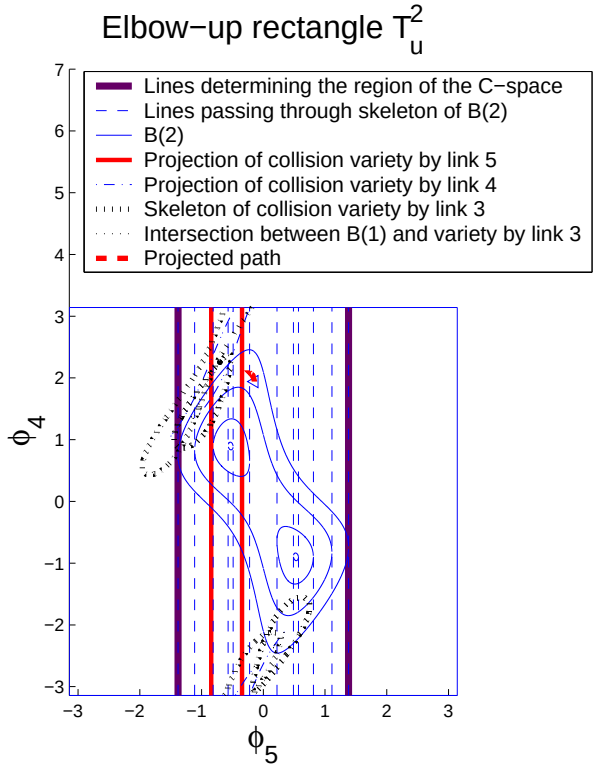

Fig. 5. The path (drawn as red dashed line) projected to T_u^2. The two triangles pointed to the left and right represent the initial and goal configurations, respectively

occurs in T_d^2 as shown in Fig. 6, but no attempt is made to connect the two graphs yet.

The next step is to "lift" the graphs so that they represent the cell structure of the two 2-tori parameterized by ϕ_{m-1} and ϕ_{m-2}. The intervals identified in the first step serve as the base manifolds for the second step. If one fixes ϕ_{m-1}, then ϕ_{m-2} lies on a circle. For the critical values of ϕ_{m-1}, the circle is drawn as a dashed vertical line (9 of the 12 are visible). Between the critical circles are two-dimensional cylindrical cells. For example, consider the two critical circles straddling $\phi_5 = 1$ in Fig. 5. This portion of C-space is a tube that is cut in four places by the projected skeleton of the boundary variety. This identifies four two-dimensional cells. The tube just to the right is cut in only two places, yielding two cells. However, in the (ϕ_{m-1},ϕ_{m-2})-space some of the cells in the two tubes are connected. After merging the connected cells, three *possibly* disconnected cells remain.

The graphs are again lifted, this time into the $(\phi_{m-1}, \phi_{m-2}, \phi_{m-3})$-space. Fig. 4 shows a cell in the (ϕ_{m-1}-ϕ_{m-2})-space. Above it is the $(\phi_{m-1}, \phi_{m-2}, \phi_{m-3})$-space with two-dimensional collision and boundary varieties. The locus of critical points are those in the intersection of the surfaces. Its projection onto the cell is the curve D, which splits the cell into two. Above each non-critical point in the two cells, there are four constraint surfaces. Assuming that the space above $B(1)(1)$ and below $B(2)(1)$ violates the loop closure constraint, then the four surfaces define two reachable cylindrical cells above the cell (a,D) and three cells above (D,b). Further the two cells bounded below by $B(2)(1)$ are connected, as are those bounded below by the surface labeled "2." Merging yields three cells in $(\phi_{m-1}, \phi_{m-2}, \phi_{m-3})$-space above the original cell in (ϕ_{m-1},ϕ_{m-2})-space.

Analyzing all adjacent cells in (ϕ_{m-1},ϕ_{m-2})-space in the same way yields all connected components of the $(\phi_{m-1}, \phi_{m-2}, \phi_{m-3})$-space, and the process continues until all connected components of dimension $m-3$ are identified.

Example further continued: A connectivity graph of $\mathcal{C}_{\text{free}}$ was constructed according to the approach described in Section VI. Then a motion planning problem was specified by the following configurations:

$$\phi_{\text{init}} = (-0.6363, -1.2183, 0.0416, 1.9416, -0.1416, \pi)$$
$$\phi_{\text{goal}} = (-0.9063, 0.8648, 0.0416, -2.0416, 0.3416, \pi).$$

One of the configurations was in the *elbow-up* torus; the other was in the *elbow-down* torus. The computed path was projected onto the two two-dimensional tori shown in Figs. 5 and 6. (Note that in these lower-dimensional spaces, one should not expect the path to jump from the *elbow-up* to the *elbow-down* spaces through the projection of $B(1)$). While it is difficult to see in a three-dimensional plot, the path in $\mathcal{C}$ crosses through the boundary variety $B(1)$. Animation of the motion in this example and others can be found in https://ai.stanford.edu/~liugf/closechain.html.

Next, we give an estimation of the complexity of the above algorithm by counting the complexity of cell decompositions at each dimension from 1 to $m-3$. Define $\text{SK}^m(i)$, $i = 0, \cdots, m-4$, the i-D skeleton of $\mathcal{C}_{\text{free}}$. Here the superscript m is specifically used to emphasize that the discussed skeleton belongs to the original m-link closed chain. Base upon the results in Section IV and V, it is

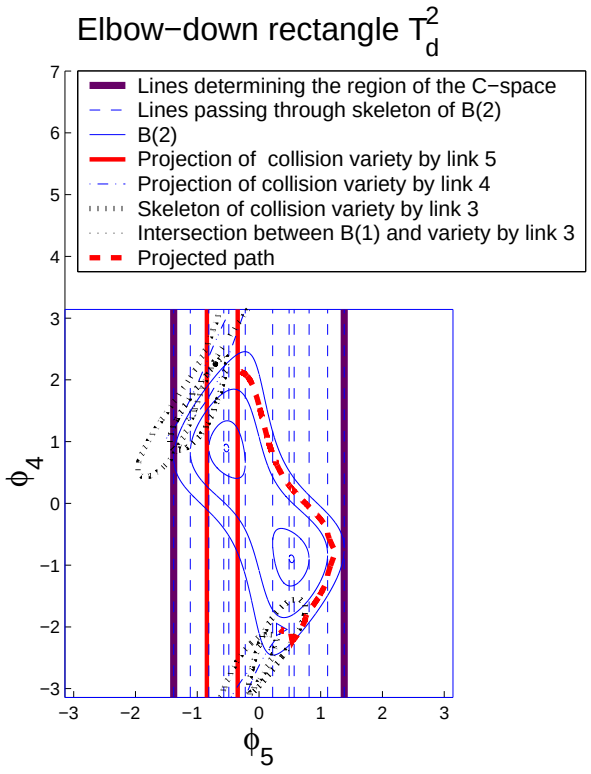

Fig. 6. The path (drawn as red dashed line) projected to T_d^2.

easy to see that $\mathrm{SK}^m(i) = B(m-3-i) \cup \Gamma(m-3-i)$ whose order, denoted as $|\mathrm{SK}^m(i)|$, is given by $C_{nm}^{m-4-i} + 2^{m-3-i} = O((nm)^{m-4-i})$ as long as $n >> m$. Since our exact cell decomposition algorithm recursively computes the decomposition of the i-D projection of $\mathcal{C}_{\text{free}}$ where i goes from 1 to $m-3$. The number of cells of the 1-D projection is easily seen to be $|\ \mathrm{SK}^m(0)\ |$, while that of the 2-D projection is given by $|\mathrm{SK}^m(0)| \cdot |\mathrm{SK}^m(1)|$ because the 2-D projection fiberates along the 1-D projection with the number of cells in each fiber determined by the number of curves in $\mathrm{SK}^m(1)$. Continuing this procedure recursively yields the following result (by direct calculation).

Proposition 1. *For a planar m-link ($m \geq 4$) closed chain moving among n point obstacles, the number of j-D ($j > 0$) cells computed in the algorithm is given by*

$$\prod_{i=0}^{j-1} |\mathrm{SK^m(i)}| = \mathrm{O}((\mathrm{nm})^{(\mathrm{m}-4)\mathrm{j}-\frac{\mathrm{j}(\mathrm{j}-1)}{2}}), \tag{4}$$

and the total number of computed cells for all dimensions is

$$\sum_{j=1}^{m-3} \prod_{i=0}^{j-1} |\mathrm{SK^m(i)}| = \mathrm{O}((\mathrm{nm})^{\mathrm{m}^2}) \tag{5}$$

as along as $n >> m$.

The final complexity of the exact cell decomposition has to take into account the effort to compute the adjacency between all $(m-3)$-D cells. However, this doesn't affect the final complexity result in Eqn. (5).

B. Exact Roadmap Algorithm

As a matter of fact, our treatment of the C-space also facilitates the development of a version of Canny's roadmap algorithm specifically for closed chains moving among point obstacles. The fact that $\mathcal{C}$ can be decomposed into an elbow-up portion and an elbow-down portion with a common boundary, and the recursive combinatorial structures of the boundary varieties $B(i)$ and the ensembles of collision varieties $\Gamma(i)$ allow us to construct the roadmaps recursively in a straightforward way.

First, consider $m >= 5$ for otherwise the problem is trivial. Notice that both $B(m-4)$ and $\Gamma(m-4)$ are a collection of 1-D curves which form a $1-D$ silhouette. So $\mathrm{SK}^m(1) = B^m(m-4) \cup \Gamma^m(m-4)$ adds into the roadmap. Here $B^m(m-4) = B(m-4)$ and $\Gamma^m(m-4) = \Gamma(m-4)$ also use the superscript m to emphasize that the curves belong to the original m-link closed-chain.

Next, consider a set of new closed chains constructed by fixing the last joint ϕ_{m-1} of the original closed chain to be one of the values in the set $\mathrm{SK}^m(0) = B^m(m-3) \cup \Gamma^m(m-3)$. Now each new closed-chain has $m-1$ links and DoFs of $m-4$, whose $1-D$ silhouette $\mathrm{SK}^{m-1}(1)$ is calculated as $B^{m-1}(m-5) \cup \Gamma^{m-1}(m-5)$ (note that $B^{m-1}(m-5) \neq B(m-5)$ and $\Gamma^{m-1}(m-5) \neq \Gamma(m-5)$ because they are now the boundary and collision varieties of the new $(m-1)$-link closed-chain), and also adds into the roadmap. The recursion continues until all closed-chains have only 2 DoFs.

Proposition 2. *For a planar m-link ($m \geq 4$) closed chain moving among n point obstacles, the number of curves in the roadmap is given by*

$$\sum_{i=m}^{5} F_i |\mathrm{SK^i(1)}| \tag{6}$$

$$F_i = \{ \begin{array}{ll} \prod_{j=m}^{i+1} |\mathrm{SK^j(0)}|, & \mathrm{i} \leq \mathrm{m}-1 \\ 1, & i = m \end{array} \}. \tag{7}$$

Compared with the cell decomposition algorithm, each item $F_k|\mathrm{SK^k}(1)|$ in the summation of Eqn. (6) is less than the corresponding item $\prod_{i=0}^{m-k} |\mathrm{SK^m(i)}|$ in the summation of Eqn. (5) by a factor of at least nm. Therefore the roadmap algorithm has much less complexity compared with the cell decomposition algorithm.

C. Resolution-complete roadmap algorithm

The exact roadmap computed for motion planning problems with point obstacles will inevitably contain segments along the C-obstacle itself, and is therefore not acceptable in practice. To solve this problem, we might compute a resolution complete roadmap algorithm by dilating point obstacles in robot workspace by an $\epsilon > 0$ (i.e. replacing each point obstacle by a small disk of radius ϵ), and approximating the disk by a set of points on its boundary circle. Here ϵ could be chosen as a positive number less than a quarter of the minimal distance among all point obstacles. One can prove the following fact.

Proposition 3. *If a given point obstacle p_i is approximated by a set of point obstacles $Q_i^\epsilon = \{q_k^i \mid q_k^i \in \mathbb{R}^2\}$ such that p_i lies in the strict interior of the convex hull $\mathrm{CONV}(Q_i^\epsilon)$ of Q_i^ϵ, then the collision variety $V_{p_i}^j$ is contained in the semi-algebraic sets cut out by the C-obstacles corresponding to Q_i^ϵ.*

Proof: see Appendix A. □

As a result, a resolution-complete complete roadmap is readily computed.

Proposition 4. *A resolution-complete roadmap for an m-link close-chain mechanism moving among $\mathcal{O} = \{p_i\}$ can be obtained from the roadmap for the same mechanism moving among $Q^\epsilon = \cup Q_i^\epsilon$, by removing those segments on the roadmap for which the mechanism intersects with at least one of the convex hulls $\mathrm{CONV}(Q_i^\epsilon)$.*

It is obvious as $\epsilon \to 0$, $Q^\epsilon \to \mathcal{O} = \{p_i\}$, and the roadmap based upon Q^ϵ converges to that base upon $\mathcal{O}$. Proposition 3 can be extended to the cases with arbitrary convex obstacles in the workspace.

Proposition 5. *If a convex obstacle $\mathcal{O}_i \subset \mathbb{R}^2$ dilates by a scale factor $\epsilon > 0$, and let the dilated obstacle be approximated by a set of points $Q_i^\epsilon = \{q_k^i \mid q_k^i \in \mathbb{R}^2\}$ on its boundary such that $\mathcal{O}_i$ lies strictly in the interior of the convex hull $\mathrm{CONV}(Q_i^\epsilon)$ of Q_i^ϵ, then the collision variety $V_{\mathcal{O}_i}^j$ consisting of all configurations for which link j intersects $\mathcal{O}_i$, is contained in the semi-algebraic sets cut out by the C-obstacles corresponding to Q_i^ϵ.*

Proposition 3, 4, and 5 allow us to construct a resolution-complete roadmap using point obstacles in $Q^\epsilon = \cup Q_i^\epsilon$, which we refer to as a dilated point obstacle set of $\mathcal{O}$. Q^ϵ is very useful for generating milestones (in $\mathcal{C}_{\text{free}}$) near $\mathcal{C}_{\text{obst}}$ for capturing narrow passages, as developed in the following section.

VII. Sampling-based Algorithm Based on Structural Information

The analysis results obtained in the subsections are useful for generating good sampling points in $\mathcal{C}_{\text{free}}$ which not only stays in the configuration space submanifold, but also are likely to capture the connectivity of the $\mathcal{C}_{\text{free}}$.

A. Random loop generator that resolves C-space bifurcations

We already know from Section III that $\mathcal{C}$ bifurcates along the boundary variety $B(1)$ where $\phi_1 = \phi_2$ or $\phi_1 = \phi_2 + \pi$. Simple local planners (such as a linear interpolation) will inevitably fail to link a pair of configurations in the two tori, respectively, even though their distance (e.g. that based upon the Euclidean metric on the chart $(\phi_3, \cdots, \phi_{m-1})$) is very small. Our method tackles this challenge with a new random loop generator.

Algorithm 1: Random loop generator algorithm

Result: $(\phi_1, \cdots, \phi_m)$ satisfies $\sum_{i=1}^m l_i \cos\phi_i = 0, \sum_{i=1}^m l_i \sin\phi_i = 0$

$\phi_m = \pi$, $\alpha_b = 0$, $i = m-1$;

$P_l = [0,0]^T$, $P_r = [l_m, 0]^T$, and $l_b = \|P_r - P_l\|$;

while $i \geq 3$ **do**

  Let $r_1 = \mathrm{CR}_{\max}^{i-2}$ and $r_2 = \mathrm{CR}_{\min}^{i-2}$;

  $b_b = 0$ and $b_s = 0$;

  if $l_i + r_1 \geq l_b$ *and* $\|l_i - r_l\| \leq l_b$ **then**

    $\beta_{\max}^1 = \arccos \frac{l_i^2 + l_b^2 - r_1^2}{2 l_i l_b}$;

    $\beta_{\min}^1 = -\beta_{\max}^1$;

    $b_b = 1$;

  end

  if $l_i + r_2 \geq l_b$ *and* $\|l_i - r_2\| \leq l_b$ **then**

    $\beta_{\max}^2 = \arccos \frac{l_i^2 + l_b^2 - r_2^2}{2 l_i l_b}$;

    $\beta_{\min}^2 = -\beta_{\max}^2$;

    $b_s = 1$;

  end

  if $b_b > 0$ *and* $b_s > 0$ **then**

    pick ϕ_i randomly from $\alpha_b + \left[\beta_{\min}^1, \beta_{\min}^2\right]$ or $\alpha_b + \left[\beta_{\max}^2, \beta_{\max}^1\right]$;

  else

    if $b_b > 0$ **then**

      pick ϕ_i randomly from $\alpha_b + \left[\beta_{\min}^1, \beta_{\max}^1\right]$;

    else

      pick ϕ_i randomly from $\alpha_b + \left[\beta_{\min}^2, \beta_{\max}^2\right]$;

    end

  end

  $P_r^{\text{old}} = P_r$, $P_r = P_r - [l_i \cos\phi_i, l_i \sin\phi_i]^T$, and $l_b = \|P_r - P_l\|$;

  $\alpha_b = \arctan 2(P_r(2) - P_l(2), P_r(1) - P_l(1))$;

end

Solving the inverse kinematics of a two-link chain (l_1, l_2) base at P_l with the end-effector location P_r yields two solutions (one in the elbow-up torus and the other in the elbow-down torus) for (ϕ_1, ϕ_2) ;

Solving the inverse kinematics of another two-link chain $(\|l_1 \pm l_2\|, l_3)$ based at P_l with the end-effector location P_r^{old} for (ϕ_1, ϕ_2, ϕ_3). These are one or two boundary configurations at which l_1 aligns with l_2;

At each iteration, this generator constructs a pair of valid samples on the configuration space manifold (i.e. satisfying the loop-closure constraints), one in the elbow-up torus and the other in the elbow-down torus. At the mean time, one or two configurations on the boundary variety $B(1)$ will also be sampled depending on the link lengths of the considered closed-chain. This algorithm requires a pre-computed data structure CR^i, $i = 1, \cdots, m-3$, for recording the radii of the set of critical circles. Given the link lengths $\{l_1, \cdots, l_m\}$ of the closed chain, CR^i are calculated as $\mathrm{CR}^i = \{l_1 \pm \cdots \pm l_i \pm l_{i+1}\}$, among which the maximal radius is denoted as $\mathrm{CR}_{\max}^i$, and the minimal one as $\mathrm{CR}_{\min}^i$. The details of this new random loop generator are summarized in Algorithm 1.

B. Sampling regions near $\mathcal{C}_{\text{obst}}$

If the workspace contains point obstacles or convex obstacles, whether or not the generated random samples are sufficient to reflect the connectivity is key to some hard motion planning problem, especially those problems in which the start and goal configurations can only be joined by the paths through some narrow passages. It has been observed by Amato et al. [28], [29] that samples around $\mathcal{C}_{\text{obst}}$ are very helpful because they improve the visibility of robots in areas between obstacles. In our cases, milestones in the regions of $\mathcal{C}_{\text{free}}$ which are close to $\mathcal{C}_{\text{obst}}$ are generated using the point obstacles in Q^{ϵ_1} (ϵ_1 is slightly greater than ϵ) which approximates $\mathcal{O}$. Configurations in $\mathcal{C}_{\text{free}}$ for which one of the links intersects a point obstacle in Q^{ϵ_1} can be regarded as the configurations close to $\mathcal{C}_{\text{obst}}$. This motivates us to develop an algorithm for sampling regions near $\mathcal{C}_{\text{obst}}$ based on Algorithm 1.

Algorithm 2: Sampling algorithm near $\mathcal{C}_{obst}$

Result: $(\phi_1, \cdots, \phi_m) \in \mathcal{C}_{\text{free}}$ satisfies $\sum_{i=1}^m l_i \cos\phi_i = 0, \sum_{i=1}^m l_i \sin\phi_i = 0$, moreover, link j intersects $q_i \in Q^{\epsilon_1}$

$P_l = [0,0]^T$, $P_r = [l_m, 0]^T$, and $l_b = \|P_r - P_l\|$;

Break the m-link closed chain into an open chain with link length $(l_1, \cdots, l_j)$ and another open chain with link length $(l_{j+1}, \cdots, l_m)$;

Replace the first chain by a closed chain of link length $(l_1, \cdots, l_{j-1}, 1/2 l_j, 1/2 l_j, l_c)$ with $l_c = \|q_i\|$;

Apply Algorithm 1 for generating a random sample for this close chain and take the coordinates $(\phi_1, \cdots, \phi_{j-1})$;

Compute $P_l = \left[\sum_{i=1}^{j-1} l_i \cos\phi_i, \sum_{i=1}^{j-1} l_i \sin\phi_i\right]^T$, and $\phi_j = \arctan(q_i(2) - P_l(2), q_i(1) - P_l(1))$;

Compute $P_l = [P_l(1) + l_j \cos\phi_j, P_l(2) + l_j \sin\phi_j]^T$, and $l_b = \|P_r - P_l\|$;

Compute $\alpha_b = \arctan 2(P_r(2) - P_l(2), P_r(1) - P_l(1))$;

Apply Algorithm 1 for generating a random sample for the closed chain $(l_{j+1}, \cdots, l_{m-1}, l_b)$ and take the coordinates $\alpha_b + (\phi_{j+1}, \cdots, \phi_{m-1})$;

Output the final sample $(\phi_1, \cdots, \phi_j, \alpha_b + \phi_{j+1}, \cdots, \alpha_b + \phi_{m-1}, \pi)$.

C. Collision checking and local planner

Combining Algorithm 1 and 2 yields an efficient algorithm for generating samples not only on the interior of $\mathcal{C}$ and the boundary variety $B(1)$, but also the region near $\mathcal{C}_{\text{obst}}$. Both algorithms rely on collision checking to filter out invalid configurations. Here a configuration $\phi \in \mathcal{C}$ is said to be collision-free if the corresponding closed chain in the workspace doesn't intersect with the dilated set $\text{CONV}(Q^\epsilon) \triangleq \cup \text{CONV}(Q_i^\epsilon)$. By triangulating $\text{CONV}(Q_i^\epsilon)$ and all links, collision checking can be performed by triangle-triangle intersection.

The next step after filtering out invalid samples is to construct a roadmap based upon the set of generated collision free samples. This requires an efficient local planner to linking nearby samples. Although $\mathcal{C}$ might not be convex, our parametrization of $\mathcal{C}$ as a pair of elbow-up and elbow-down $(m-3)$-D torii allows us to construct efficient local planners based upon a minimal-distance joint-interpolation motion of $\text{CH}_2(1)$ based at $P_r = [l_m, 0]^T$, and an *accordion motion* of $\text{CH}_1(1)$ based at $P_l = [0,0]^T$.

Given a pair of configurations $\phi^1 = (\phi_1^1, \phi_2^1, \psi^1)$ and $\phi^2 = (\phi_1^2, \phi_2^2, \psi^2)$ of the original closed chain where $\psi^i = (\phi_3^i, \cdots, \phi_{m-1}^i)$, $i = 1, 2$, are the corresponding pair of configurations for $\text{CH}_2(1)$. If $\phi_2^1 - \phi_1^1$ has same sign as $\phi_2^2 - \phi_1^2$ (i.e., they belong to the same torus), a local planner for $\text{CH}_2(1)$ is constructed as

$$\psi(t) = \psi^1 + \delta\psi * t, \quad t \in [0,1]\,, \tag{8}$$

where $\delta\psi$ is the vector $\psi^2 - \psi^1$ projected (through modular operation) to the interval $[-\pi, \pi]^{m-3}$. Under $\psi(t)$ the end-effector of $\text{CH}_2(1)$ follows a smooth curve $\gamma(t) = f_{2,1}(\psi(t)) \in \mathbb{R}^2$ between $\gamma(0) = f_{2,1}(\psi^1) \in \mathbb{R}^2$ and $\gamma(1) = f_{2,1}(\psi^2) \in \mathbb{R}^2$ (Recall that $f_{2,1}$ is the forward kinematic map of $\text{CH}_2(1)$). Moreover $r_{\min}^2 \le \|\gamma(t) - P_r\| \le r_{\max}^2, \forall t$, with $r_{\min}^2 = \min\{\mid l_3 \pm \cdots \pm l_{m-1} \mid\}$ and $r_{\max}^2 = \sum_{i=3}^{m-1} l_i$. If every point in $\gamma(t)$ can be closed by $\text{CH}_1(1)$, then we might apply the inverse kinematics map $f_{1,1}^{-1}$ of $\text{CH}_1(1)$ to compute an interpolation which is "compliant" with $\gamma(t)$. $f_{1,1}^{-1}(\gamma(t))$ is referred to as an accordion move if the same sign as (ϕ_1^1, ϕ_2^1) (also (ϕ_1^2, ϕ_2^2)) is adopted in the calculation of the inverse kinematics for every point in $\gamma(t)$.

Theorem 1. *Let $r_{\min}^1 = \|l_1 - l_2\|$, and $r_{\max}^1 = l_1 + l_2$. Suppose the start and end points of $\gamma(t)$ lies in the strict interior of the workspace of $\text{CH}_1(1)$, i.e., there exists $0 < \delta r < \frac{1}{2}(r_{\max}^1 - r_{\min}^1)$ such that $r_{\min}^1 + \delta r < \|\gamma(0) - P_l\| < r_{\max}^1 - \delta r$ and $r_{\min}^1 + \delta r < \|\gamma(1) - P_l\| < r_{\max}^1 - \delta r$. Then there exists an $\epsilon > 0$ such that as long as $\|\delta\psi\| < \epsilon$, $r_{\min}^1 < \|\gamma(t) - P_l\| < r_{\max}^1$ for all $t \in [0,1]$. If only one end of $\gamma(t)$ lies in the strict interior while the other end lies on a critical circle, then the same inequality holds for all $t \in (0,1)$.*

Proof: See Appendix B. □

Theorem 1 shows that as long as ψ^1 and ψ^2 are sufficiently close and have same sign, then there is always an accordion move for $\text{CH}_1(1)$ that closes the loop at every $t \in [0,1]$. However if ϕ^1 and ϕ^2 have different sign for $\text{CH}_1(1)$, then the above local planner will fail. Fortunately, the milestones generated from Algorithm 1 contain samples exactly on the boundary variety $B(1)$, which can be used for bridging pairs of configurations in different torii. With these samples the resulting roadmap is able to overcome the difficulties from the bifurcations of $\mathcal{C}_{\text{free}}$.

D. Experimental Results

Our method was implemented in Matlab and tested for many planning problems (with number of links from 5 to 50). All matlab programs were run under Windows 10 and Intel Core *i*7. Our software can be downloaded from https://ai.stanford.edu/~liugf/closechain.html, in which animation videos can be found for all the examples discussed below.

The first simulation result is about a 6-bar closed chain moving among 6 point obstacles (see Fig. 7-(a)), same mechanism but with only 2 point obstacles has already been studied in the previous examples). This example is quite challenging. First the start and goal configurations

$$(-0.6363, -1.2183, 0.0416, 1.9416, -0.1416, \pi)$$
$$(-0.9063, 0.8648, 0.0416, -2.0416, 0.3416, \pi)$$

lie in two different torii. This means any feasible path

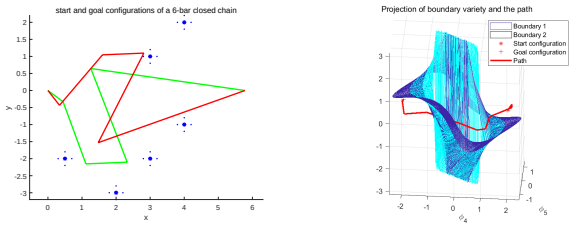

Fig. 7. (a): start (in green) and goal (in red) configurations of a 6-bar closed chain, original point obstacle set (blue star) and the dilated point obstacle set (blue dot); (b): 3-D view of the C-space, including two pieces of the boundary variety $B(1)$, shown as two bitorii (one in blue, and the other in cyan), and the robot path (in red)

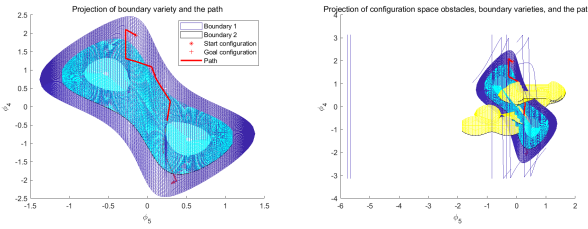

Fig. 8. (a): Projection of the C-space; (b): Projection of $\mathcal{C}_{\text{obst}}$

between them will inevitably intersect the boundary variety $B(1)$. A 3-D view of $\mathcal{C}$ as well as its boundary variety $B(1)$ is given in Fig. 7-(b). Second, given the tight layout of point obstacles and the given start and goal configurations, the robot will have to go through some narrow passages created by C_{obst}. A 2-D view of $\mathcal{C}$ and $\mathcal{C}_{\text{obst}}$ is illustrated in Fig. 8. Note that in Fig. 8-(b) some vertical lines (in blue) are projection of $V^5_{p_i}$, and others (also in blue) are simply 2π jumps for joining two curve segments on top and bottom of the 2-D torus. The latter collision varieties are projection of $V^4_{p_i}$. Finally those in yellow are projection of $V^3_{p_i}$. Our software generates 535 random samples (in less than a minute) which satisfy the loop-closure constraints and are collision-free. We use the joint space Euclidean distance filtered by 2π to measure the closeness between pairs of random samples. The local planner discussed in the previous subsection will be applied to join the closest 6 (reconfigurable) samples of each milestone until every milestone and its neighbors are examined. The resulting roadmap is shown in Fig. 9. The motion planning problem is solved by connecting the start and goal configurations to the graph vertices with the same local planner, followed by a minimal-distance search. Fig. 10, 11, and 12 show the resulting path. Notice that at the end of the first path segment and the beginning of the second path segment (as well as the last segment), the robot goes through the sample which lies in the collision varieties of the point obstacle (shown as blue dot) of the dilated set of one original point obstacle (shown in as blue star). These are crucial for get through the narrow passages without colliding with the original point obstacle. In the middle of path segment 5 in Fig. 12-(a), the robot finishes a motion that crosses $B(1)$ from the elbow-up torus to the elbow-down torus. The sampled configuration on $B(1)$ is necessary for achieving this motion

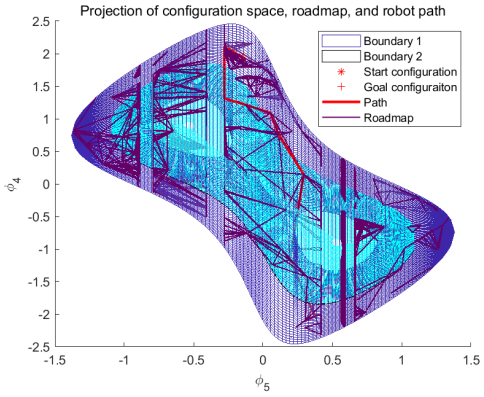

Fig. 9. Projection of the computed roadmap (in brown) and robot path (in red)

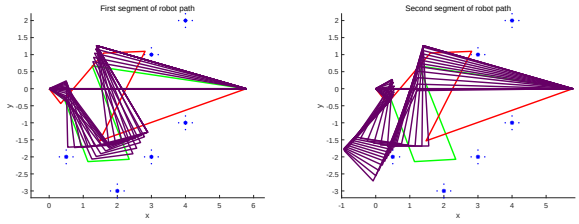

Fig. 10. (a): First segment of robot path; (b): Second segment of robot path

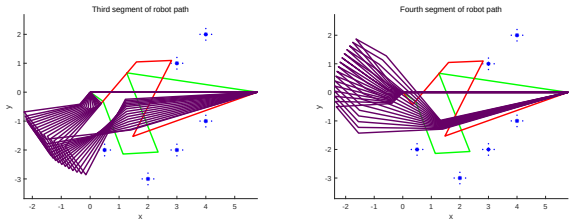

Fig. 11. (a): Third segment of robot path; (b): Fourth segment of robot path

Next we apply our algorithm to the example of a 10-bar closed-chain moving among 10 point obstacles. The link lengths are $\{1.2, 2.0, 0.5512, 1.9457, 1.2131, 2.9482, 4.5684, 0.3, 0.3, 8.5815\}$, and the start and goal configurations are $\{0.6669, -0.3802, -0.6014, -1.1834,$

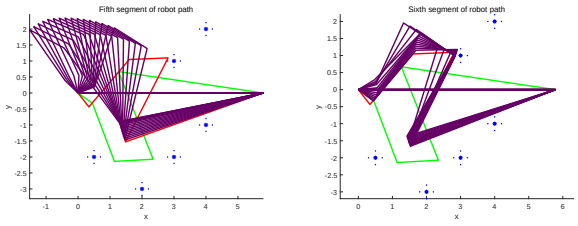

Fig. 12. (a): Fifth segment of robot path; (b): Last segment of robot path

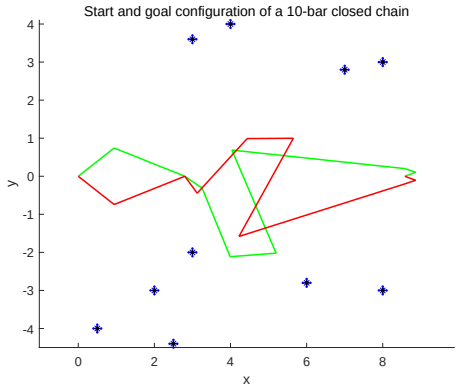

Fig. 13. Start (in green) and goal (in red) configurations of a 10-bar closed-chain moving among 10 point obstacles

$0.0765, 1.9765, -0.1067, -0.3255, -2.7811, 3.1416\}$ and $\{-0.6669, 0.3802, -0.9412, 0.8299, 0.0067, -2.0765, 0.3067, 0.3255, 2.7811, 3.1416\}$, respectively. Our algorithm generates over 3000 milestones for the roadmap, and the resulting path is shown in Fig. 14, 15, and 16. In this example the mechanism crosses the boundary variety in Fig. 14-(a), and has to move through several narrow passages in Fig. 15 and 16 toward far left for adjusting the sign of link 8 and 9 to the desired one before arriving the goal configuration.

VIII. Conclusion

This paper presents a framework that employs the structural information of the C-space $\mathcal{C}$ for solving the motion planning problems of planar closed chains. This framework combines the results on the topology of C-space of planar closed chains and the combinatorial structure of their boundary variety $B(1)$ and collision varieties $\mathcal{C}_{\text{obst}}$. First, $\mathcal{C}$ is covered using only two charts, each imbedded in an $(m\text{-}3)$-dimensional torus. The connectivity between the two torii is completely determined by $B(1)$. Second, the structure of $B(1)$ and $\mathcal{C}_{\text{obst}}$ is analyzed using the C-spaces of a recursively constructed set of closed chains. These structural information is used to explicitly construct exact cell decomposition and roadmap for $\mathcal{C}_{\text{free}}$. For the latter one, we also provide a resolution-complete version using a dilated set of point obstacles. Finally we develop a refined random loop generator algorithm that generates samples in both $\mathcal{C}_{\text{free}}$ and $B(1)$, as well as another sampling

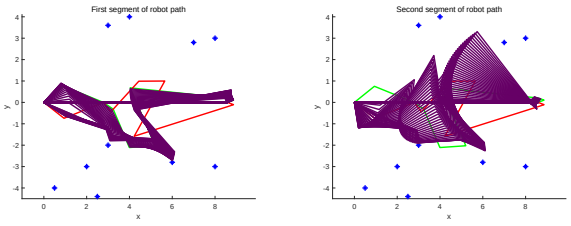

Fig. 14. (a): First segment of robot path; (b): Second segment of robot path

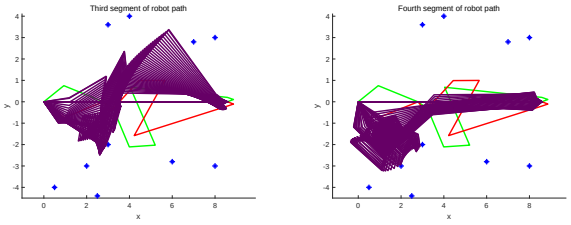

Fig. 15. (a): Third segment of robot path; (b): Fourth segment of robot path

algorithm that generates collision-free samples near $\mathcal{C}_{\text{obst}}$. This new algorithm is able to solve the challenges of C-space bifurcations and narrow passages, as demonstrated by examples, among which some are very difficult to solve with traditional approaches.

Acknowledgment

The authors would like to thank Jim Milgram for introducing them to many of the ideas that led to the results obtained.

Appendix A
Proof of Proposition 3

Recall $V^j_{p_i}$ is the set of configurations for which link j intersects p_i. Consider three cases: (1) $j \in \{3, \cdots, m-1\}$; (2) $j = 2$; (3) $j = 1$.

Case (1): suppose p_i stays in the strict interior of the workspace of the right open chain $(l_3, \cdots, l_{m-3})$ based at $(l_m, 0)$, and can be reached by link j at a configuration $\psi = (\phi_3, \cdots, \phi_{m-1})$. ψ lies in the strict interior of the interval between $\psi^1 = (\phi_3, \cdots, \phi_{j-1}, \phi_j^{\min}, \phi_{j+1}, \cdots, \phi_{m-1})$ and $\psi^2 = (\phi_3, \cdots, \phi_{j-1}, \phi_j^{\max}, \phi_{j+1}, \cdots, \phi_{m-1})$. Notice that link j of the right open chain intersects one of the point obstacles in the dilated set Q^ϵ at both ψ^1 and ψ^2. Because ϵ is a sufficient small positive number, the existence of the interval $\left[\phi_j^{\min}, \phi_j^{\max}\right]$ that contains ϕ_j is guaranteed. If p_i stays on the boundary of the workspace of the right open chain, then it must lie in the strict interior of the workspace of the left open chain (l_1, l_2) for otherwise, there exists only one configuration for which link j intersects p_i and this configuration lies in the boundary of $\mathcal{C}$ (regarded as trivial).

Case (2),(3): If p_i lies in the strict interior of the workspace of the left open chain. Then at least one of $V^j_{p_i}$,

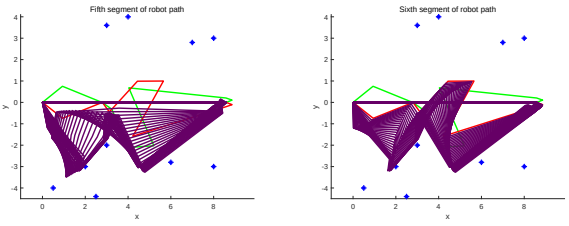

Fig. 16. (a): Fifth segment of robot path; (b): Last segment of robot path

$j = 1, 2$, is non-empty. Using the same argument, each collision configuration (ϕ_1, ϕ_2) (for which the left open chain intersects p_i) lies in the interval between (ϕ_1^1, ϕ_2^1) and (ϕ_2^1, ϕ_2^2). At these two configurations either link 1 or link 2 intersects one of the point obstacles in Q^ϵ.

Appendix B
Proof of Theorem 1

We first prove that $r^1_{\min} < \|\gamma(t) - P_l\|$, and the fact $\|\gamma(t) - P_l\| < r^1_{\max}$ can be proved in the same manner. We have

$$\begin{aligned} \|\gamma(t) - P_l\| &= \|f_{2,1}(\psi(t)) - P_l\| \\ &= \|f_{2,1}(\psi(t)) - f_{2,1}(\psi^1) + f_{2,1}(\psi^1) - P_l\| \\ &\geq \|f_{2,1}(\psi^1) - P_l\| - \|f_{2,1}(\psi(t)) - f_{2,1}(\psi^1)\| \\ &\geq r^1_{\min} + \delta r - \|Jf_{2,1}(\psi(t_1))\|\|\psi(t) - \psi^1\| \end{aligned}$$

for some $t_1 \in [0, 1]$. Because the interval $[0, 1]$ is compact, $\|Jf_{2,1}(\psi(t_1))\|$ is bounded from above by a positive value $\eta > 0$. Therefore as long as $\|\psi(t) - \psi^1\| \leq \|\psi^2 - \psi^1\| < \epsilon < \frac{\delta r}{\eta}$, then $r^1_{\min} < \|\gamma(t) - P_l\|$.

References

[1] G. Collins, *Quantifier Elimination for Real Closed Fields by Cylindrical Algebraic Decomposition.* Proceeding, Second GI Conference on Automata Theory and Formal Languages, Vol. 33, PP. 134-183, 1975, Springer-Verlag.

[2] M. Kapovich and J. Millson, *On the moduli spaces of polygons in the Euclidean plane.* Journal of Differential Geometry, Vol. 42, PP. 133-164, 1995.

[3] J.-C. Hausmann and A. Knutson, *The cohomology ring of polygon spaces.* Ann. Inst. Fourier, Vol. 48, PP. 281-321, 1998.

[4] Y. Kamiyama, M. Tezuka, and T. Toma, *Homology of the Configuration Spaces of Quasi-Equilateral Polygon Linkages.* Transactions of the American Mathematical Society, Vol. 350, No. 12, PP. 4869-4896, 1998.

[5] J. Hopcroft and G. Wilfong, *On the motion of objects in contact.* Int. J. Robotics Research, Vol. 4, 1986, PP. 32-46.

[6] J.F. Canny, *The Complexity of Robot Motion Planning.* Cambridge, MA: MIT Press, 1988.

[7] J.C. Latombe, *Robot Motion PLanning.* Kluwer Academic Publishers, 1992.

[8] J. Schwartz, J. Hopcroft, and M. Sharir, *Planning, Geometry, and Complexity of Robot Motion.* Ablex, 1987.

[9] L.E. Kavraki, P. Švestka, J.C. Latombe, and M.H. Overmars, *Probablistic Roadmaps for path planning in high-dimensional configuration space.* IEEE Transactions on Robotics and Automation, 12(4):566-580, 1996.

[10] S. M. LaValle and J. J. Kuffner, *Rapidly-exploring random trees: Progress and prospects.* In B. R. Donald, K. M. Lynch, and D. Rus, editors, Algorithmic and Computational Robotics: New Directions, pages 293-308, A K Peters, Wellesley, MA, 2001.

[11] S. R. Lindemann and S. M. LaValle, *Current issues in sampling-based motion planning.* In P. Dario and R. Chatila, editors, Proc. Eighth Int'l Symp. on Robotics Research. Springer-Verlag, Berlin, 2004. To appear.

[12] J. Yakey, S. M. LaValle, and L. E. Kavraki, *Randomized path planning for linkages with closed kinematic chains.* IEEE Transactions on Robotics and Automation, 17(6):951–958, December 2001.

[13] J. Cortes, *Motion planning algorithms for general closed-chain mechanisms.* Doctorat, Institut National Polytechnique, Toulouse, December 16, 2003, 160p.

[14] K.L. Ting. Mobility criteria of single loop n-bar linkages. *Trans. ASME, Journal of Mechanisms, Transmissions and Automation in Design*, 111(4):504–507, December 1989.

[15] K.L. Ting and Y.W. Liu. Rotatability laws for n-bar kinematic chains and their proof. *ASME Journal of Mechanical Design*, 113(1):32–39, 1991.

[16] J.T. Schwartz and M. Sharir, *On the piano movers II. General techniques for computing topological properties on real algebraic manifolds.* Adv. Appl. Math., vol.4, PP. 298-351, 1983.

[17] L. Han and N.M. Amato, *A kinematics-based probabilistic roadmap method for closed chain systems.* in Algorithmic and Computational Robotics: New Directions, B.R. Donald, K.M. Lynch, and D. Rus, Eds. AK Peters, Wellesley, PP. 233-246, 2001.

[18] J.C. Trinkle and R.J. Milgram, *Complete Path Planning for Closed Kinematic Chains with Spherical Joints.* International Jounral of Robotics Research, 21(9):773-789, December, 2002.

[19] G.F. Liu, J.C. Trinkle, R.J. Milgram, *Complete Path Planning for Planar 2-R Manipulators With Point Obstacles.* Proceedings of IEEE International Conference on Robotics and Automation, 3263-3269, 2004.

[20] G.F. Liu, J.C. Trinkle, R.J. Milgram, *Complete Path Planning for Planar 3R-Manipulators Among Point Obstacles.* To appear in Proceedings of WAFR 2004.

[21] D. Halperin, "Algorithmic Motion Planning via Arrangements of Curves and Surfaces", Doctoral Dissertation, Tel-Aviv University, Israel.

[22] Beobkyoon Kim, Terry Taewoong Um, Chansu Suh and F. C. Park, *Tangent bundle RRT: A randomized algorithm for constrained motion planning.* Robotica, 34, pp 202-225 doi:10.1017/S0263574714001234.

[23] G. Liu, Y. Lou, and Z. Li, *Singularities of parallel manipulators: a geometric treatment.* IEEE Transactions on Robotics and Automation, vol. 19, no. 4, pp. 579ÍC594, 2003.

[24] F. C. Park and J. W. Kim, *Singularity analysis of closed kinematic chains.* hskip 1em plus 0.5em minus 0.4em Journal of Mechanical Design, Transactions of the ASME, vol. 121, no. 1, pp. 32ÍC38, 1999.

[25] N. Shvalb, M. Shoham, H. Bamberger, and D. Blanc, *Topological and kinematic singularities for a class of parallel mechanisms.* Mathematical Problems in Engineering, vol. 2009, Article ID 249349, 12 pages, 2009.

[26] Zhang K., Muller A., Dai J.S., *A Novel Reconfigurable 7R Linkage with Multifurcation.* In: Ding X., Kong X., Dai J. (eds) Advances in Reconfigurable Mechanisms and Robots II. Mechanisms and Machine Science, vol 36. Springer.

[27] MÍźller A., Zhang K., Dai J.S. *Analysis of the Motion Mode Change of a Metamorphic 8R Linkage.* In: Ding X., Kong X., Dai J. (eds) Advances in Reconfigurable Mechanisms and Robots II. Mechanisms and Machine Science, vol 36. Springer.

[28] Rodriguez S, Xinyu Tang, Lien Jyh-Ming, Amato Nancy. *An obstacle-based rapidly-exploring random tree.* Proceedings - IEEE International Conference on Robotics and Automation. 2006. 895 - 900. 10.1109/ROBOT.2006.1641823.

[29] N. Amato, O. Bayazit, L. Dale, C. Jones, D. Vallejo, *OBPRM: An obstacle-basedPRM for 3D workspaces.* in: P.K. Agarwal, L.E. Kavraki, M.T. Mason (eds.), Robotics: The algorithmic perspective, A.K. Peters, Natick, 1998, pp. 155ÍC168.